electronics

MDPI

Article

Gallium Nitride Normally Off MOSFET Using Dual-Metal-Gate Structure for the Improvement in Current Drivability

Young Jun Yoon [1], Jae Sang Lee [1], Dong-Seok Kim [1], Jung-Hee Lee [2] and In Man Kang [2,*]

[1] Korea Multi-purpose Accelerator Complex, Korea Atomic Energy Research Institute, Gyeongju 38180, Korea; yjyoon@kaeri.re.kr (Y.J.Y.); jslee8@kaeri.re.kr (J.S.L.); dongseokkim@kaeri.re.kr (D.-S.K.)

[2] School of Electronics Engineering, Kyungpook National University, Daegu 41566, Korea; jlee@ee.knu.ac.kr

* Correspondence: imkang@ee.knu.ac.kr; Tel.: +82-053-950-5513

Received: 3 August 2020; Accepted: 28 August 2020; Published: 30 August 2020

Abstract: A gallium nitride (GaN)-based normally off metal–oxide–semiconductor field-effect transistor (MOSFET) using a dual-metal-gate (DMG) structure was proposed and fabricated to improve current drivability. Normally off operation with a high V_{th} of 2.3 V was obtained using a Cl_2/BCl_3-based recess etching process. The DMG structure was employed to improve current characteristics, which can be degraded by recess etching. The I_D and g_m of a DMG-based device with nickel (Ni)-aluminum (Al) were improved by 42.1% and 30.9%, respectively, in comparison to the performances of a single-metal-gate-based device with Ni because the DMG structure increased electron velocity in the channel region. This demonstrates that the DMG structure with a large work-function difference significantly improves the carrier transport efficiency. GaN-based recessed-gate MOSFETs based on the DMG structure hold promising potentials for high-efficiency power devices.

Keywords: GaN; recessed-gate; normally-off; dual-metal-gate structure

1. Introduction

Gallium nitride (GaN)-based electronics have huge potentials for high-efficiency power electronic applications [1,2] because a two-dimensional electron gas (2DEG) with high electron density and high electron mobility obtained by AlGaN/GaN heterostructures achieves low switching and conduction losses [3,4]. Additionally, GaN-based electronic devices can obtain a higher breakdown voltage than silicon (Si)-based devices because GaN has a higher critical electric field than Si [5]. GaN-based high-electron-mobility transistors (HEMTs) or metal–insulator–semiconductor HEMTs (MIS-HEMTs) show a normally on operation with a negative threshold voltage (V_{th}) due to the high electron density of 2DEGs. A normally off operation with a high positive V_{th} is needed to guarantee safe operation in power switching applications [6]. Various structures and fabrication processes such as the recessed-gate [7–11], p-GaN gate [12,13], cascade configuration [14], and fluorine plasma treatment [15,16] have been presented to realize the normally off operation of GaN-based electronic devices. Among the above-stated structures, the recessed-gate devices can achieve a high V_{th} and wide range of gate drive voltages (V_G), as well as low gate leakage current. However, the recess etching, which partially or fully removes the aluminum GaN (AlGaN) layer for normally off operation, significantly degrades current performances due to the reduction in field-effect mobility [8,17]. Although several processes such as tetramethylammonium hydroxide (TMAH) treatment [18] and O_2-BCl_3 digital etching processes [19] have been employed to minimize etching damage, achieving simultaneously excellent current characteristics, as well as a high V_{th}, remains a difficult problem. There is a trade-off between the on-state current and V_{th} because these characteristics are both affected by recess depth [20].

Recently, recessed-gate metal–oxide–semiconductor field-effect transistors (MOSFETs) combined with novel structures such as a regrown AlGaN barrier [11] and double AlGaN barrier [21] were fabricated using epitaxial technology to satisfy both current performance and V_{th}. However, performances of the devices depended on sensitive epitaxial technology and needed epitaxial equipment.

In this work, we applied a dual-metal-gate (DMG) structure in a recessed-gate GaN-based MOSFET to achieve improved current performances and high V_{th}. The DMG structure has been proposed in Si MOSFETs and can enhance electron velocity due to the distribution impact of the electric field [22]. In addition, we confirmed that the DMG structure enhanced performances of GaN-based MIS-HEMTs [23,24] as previous works. The present work shows the effects of the DMG structure on performances of the recessed-gate MOSFETs. We fabricated a recessed-gate MOSFET with a DMG structure to demonstrate the reduction in channel resistance increased by recess etching. The impacts of the DMG structure on electron density, energy band diagram, electric field, and electron velocity under the recessed-gate region were analyzed using a technology computer-aided design (TCAD) simulator. The current characteristics of fabricated DMG-based devices were compared to those of single-metal-gate (SMG)-based devices to demonstrate the effects of the DMG structure. Furthermore, the effect of the work-function difference in the DMG structure on current characteristics was investigated.

2. Structure and Fabrication

Figure 1a,b shows the schematic cross-sections of the SMG- and DMG-based devices, respectively. The SMG-based device is the conventional recessed-gate device with a nickel (Ni) metal gate. The DMG-based device consists of Ni at the source-side gate (M1) and aluminum (Al) or titanium (Ti) at the drain-side gate (M2). The Ni with a high work function was designed on the source-side to obtain a high V_{th} because the potential barrier height formed by the source-side gate determined V_{th} [25]. To form the potential difference in the channel region, Al or Ti with a low work function was employed in the M2 region.

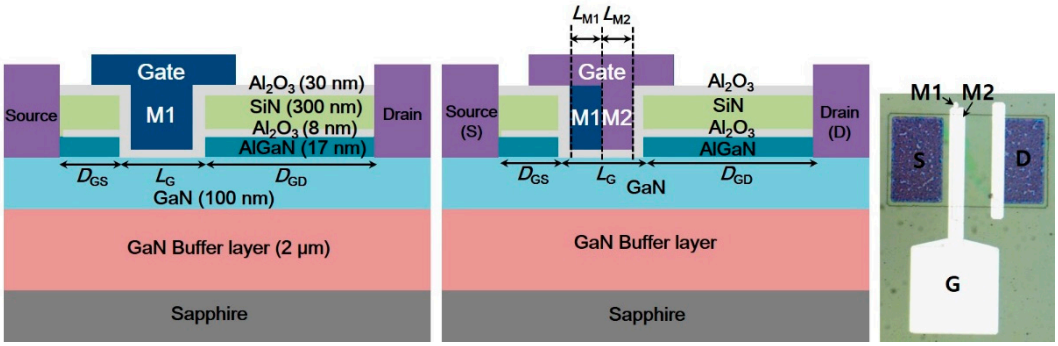

Figure 1. Schematic cross-sections of the recessed-gate GaN metal–oxide–semiconductor field-effect transistor (MOSFET) with (**a**) the single-metal-gate (SMG) and (**b**) dual-metal-gate (DMG) structures. (**c**) Optical microscope image of the fabricated DMG-based device.

The SMG- and DMG-based devices were fabricated on an identical AlGaN/GaN heterostructure, which was grown by the metal–organic chemical vapor deposition (MOCVD) technique on a *c*-plane sapphire substrate. The AlGaN/GaN heterojunction formed a 2DEG with an electron density of 1.0×10^{13} cm^{-2} and electron mobility of 1600 cm^2/V·s, which were estimated using Hall measurement at room temperature. The epitaxial layers consisted of a 2 μm-thick GaN buffer layer, 100 nm-thick undoped GaN channel layer, and 17 nm-thick AlGaN layer. The Al composition in the AlGaN layer was 0.25. The fabrication process started with mesa etching using Cl_2/BCl_3 plasma-based inductively coupled plasma (ICP) to isolate the devices. After the mesa etching, an 8 nm-thick Al_2O_3 layer as

a protection layer for thermal annealing was deposited using atomic layer deposition (ALD). Then, Au/Ni/Al/Ti/Si metal layers were deposited and annealed at 800 °C for 30 s in a dinitrogen (N_2) ambient to form ohmic contact in the source and drain regions. After the ohmic process, a 300 nm-thick SiN layer was additionally deposited using plasma-enhanced chemical vapor deposition (PECVD) at 370 °C to form a field-plate structure. The SiN, Al_2O_3, and AlGaN layers were sequentially etched using a buffered oxide etch (BOE) solution and Cl_2/BCl_3 plasma-based ICP for the normally off operation. Here, the channel resistance can be increased by the surface damage, which was obtained by etching the AlGaN layer. A 30 nm-thick Al_2O_3 layer as a gate dielectric was deposited using ALD. The gate metal was formed using an electron beam evaporator. The gate metal of the SMG structure consisted of the Ni/Al/Ni metal layer. For the DMG structure, the Ni and Ti/Ni or Al/Ni metal layers were deposited as the M1 and M2, respectively. The DMG structure was fabricated through two photolithography and two metal deposition processes. Finally, the post metallization annealing process was performed to improve the quality of the metal and Al_2O_3 interface [26].

3. Results and Discussion

Figure 2a shows the transfer characteristics of the SMG and DMG-based devices. The DMG-based device with Ni-Ti metal exhibited a higher I_D and g_m than the SMG-based device with Ni metal. This result indicates that the DMG structure reduced the channel resistance because of the improved electron velocity. In addition, the DMG structure can improve the channel mobility, which was affected by traps in the Al_2O_3 gate dielectric layer. The electron beam evaporation of Ni in the SMG structure needs higher beam energy compared to Ti, resulting in the high damage in the Al_2O_3 gate dielectric layer. The damaged gate dielectric layer induced traps [27,28], which degenerated the channel mobility [29]. In terms of fabrications, as the DMG structure received relatively small damage, the DMG structure had a positive impact on channel mobility. The V_{th} of the SMG- and DMG (Ni-Ti)-based devices was 2.66 V and 2.3 V, respectively. Although the V_{th} of the DMG-based device was slightly decreased, the normally off operation was obtained by the potential energy barrier, which was formed by the M1 of the DMG structure. In terms of the off-state leakage current, the leakage current of the DMG-based device was slightly higher than that of the SMG-based device, as shown in Figure 2b. This is due to the potential energy barrier suppressing the leakage current. As shown in Figure 2c, the DMG structure also reduced static on-resistance (R_{on}) by increasing the maximum I_D ($I_{D,max}$). This result showed that the DMG structure significantly improved R_{on} and $I_{D,max}$.

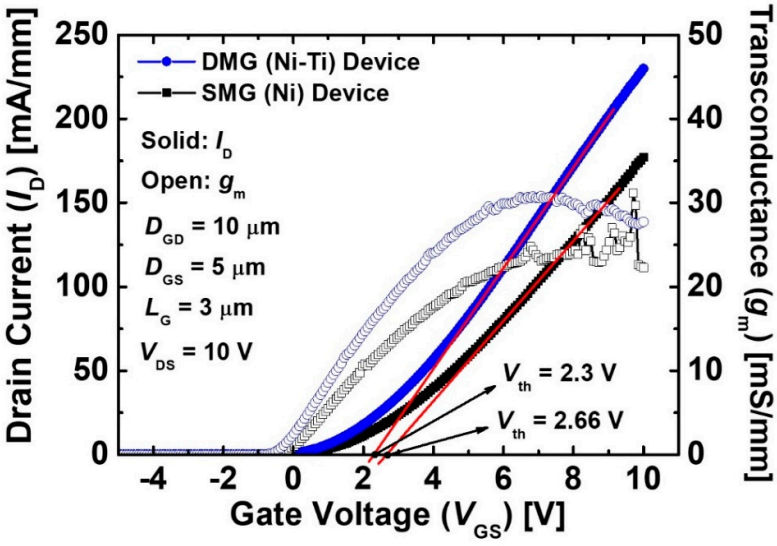

(**a**)

Figure 2. *Cont.*

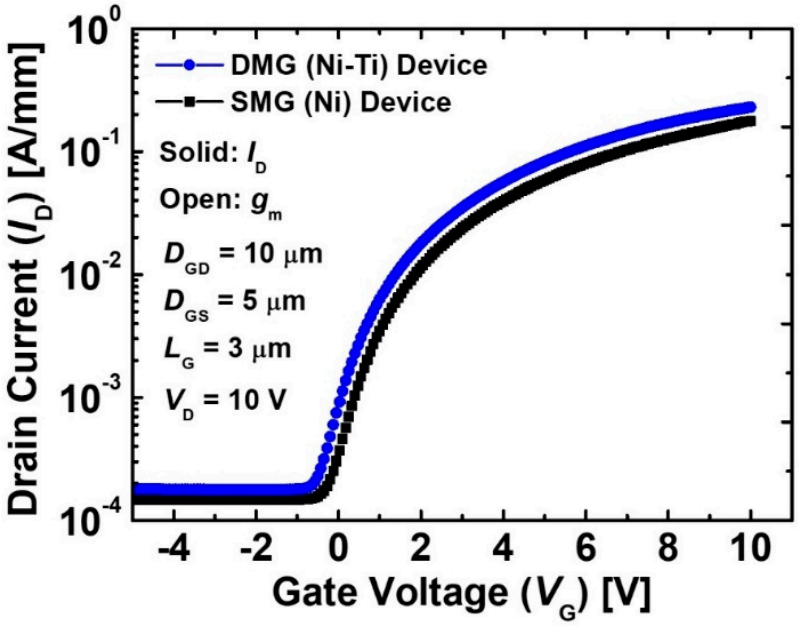

(**b**)

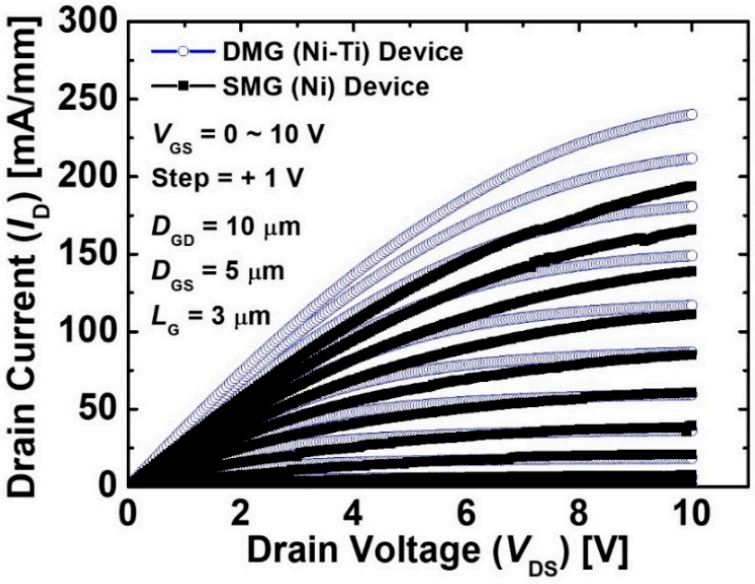

(**c**)

Figure 2. (**a**) Linear scale I_D and g_m, (**b**) logarithmic scale I_D, and (**c**) output characteristics of the SMG and DMG-based devices. The L_G, D_{GD}, and D_{GS} of both devices were 3 μm, 10 μm, and 5 μm, respectively. The M1 and M2 in the DMG structure consist of Ni and Ti, respectively.

We simulated the SMG- and DMG-based devices using the TCAD simulator [30] to investigate the effects of DMG structure on electron density, energy band, electric field, and electron velocity at the recess region. The simulation was performed with various physical models for GaN and AlGaN materials, including polarization, low- and high-field-dependent mobility, and Schockley–Read–Hall (SRH) recombination models. Simulation results of electron density at a zero bias (V_G = 0 V and V_D = 0 V) of the SMG- and DMG-based device are shown in Figure 3a. Both devices achieved a low electron density under the gate region at V_G = 0 V because the GaN channel layer was fully depleted by the high work-function of Ni(M1). Figure 3b shows the energy band diagrams at the off-state

condition (V_G = 0 V and V_D = 10 V) of the SMG- and DMG-based devices. The electron potential barrier was maintained under the M1 gate region due to the M1 in the DMG structure, even though a V_D = 10 V was applied. As the effect of the M1 gate region on the electron potential barrier is dominant, the DMG-based device can obtain normally off operation with a positive V_{th}. The electron potential distribution formed by the DMG structure affected the electric field distribution at the interface of M1/M2 and the drain-side gate edge. As shown in Figure 3c, while the electric field peak at the drain-side gate edge of the DMG-based device was smaller than that of the SMG-based device, the electric field peak at the interface of M1/M2 increased, resulting in the increase in electron velocity at the recess region because electron velocity is dependent on the electric field [31,32], as shown in Figure 3d. Consequently, the current characteristics can be improved by the DMG structure because, as the electron velocity increases, carrier transport efficiency is enhanced.

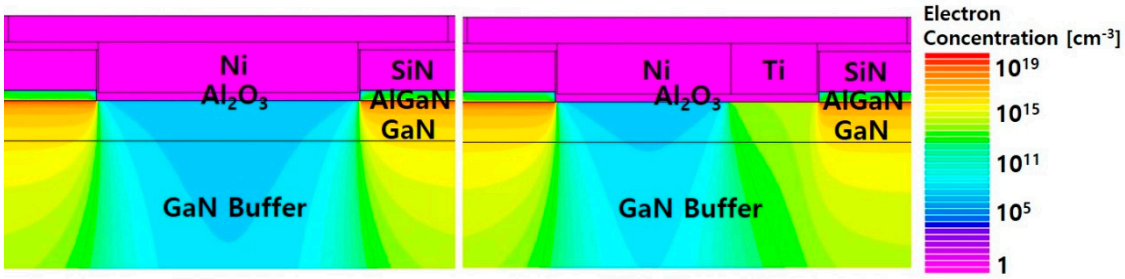

(**a**)

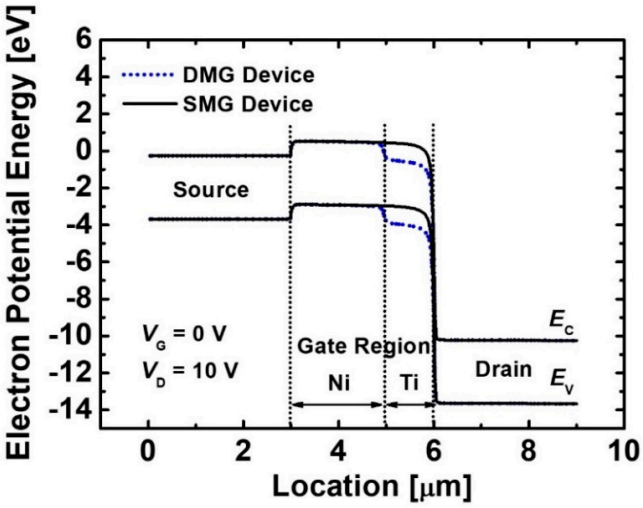

(**b**)

Figure 3. *Cont.*

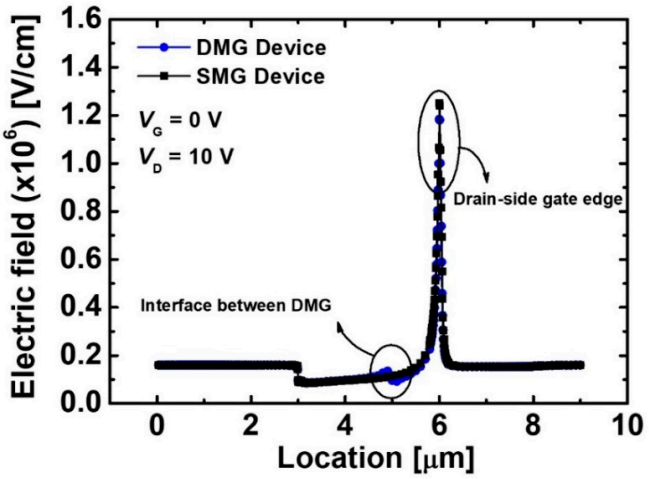

(**c**)

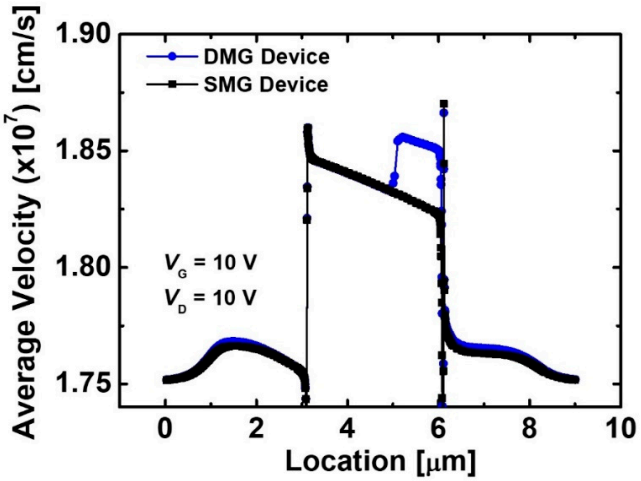

(**d**)

Figure 3. Technology computer-aided design (TCAD) simulated results of the devices with the SMG (Ni) and DMG (Ni-Ti) structures. (**a**) Electron density at zero bias, (**b**) energy band diagrams at the off-state, (**c**) electric field at the off-state, and (**d**) electron velocity at the on-state. The total L_G of the SMG- and DMG-based devices was 3 μm. The L_{M1} and L_{M2} of the DMG-based device are 2 μm and 1 μm, respectively.

Figure 4a shows the transfer characteristics of the SMG- and DMG-based devices with different L_G at a V_D = 10 V. We compared the DMG (Ni and Ti) and SMG (Ni) devices to investigate effects of the DMG with different L_G on current performance. The DMG-based device exhibited a higher I_D and g_m than the SMG-based device, even though the DMG-based device with L_G = 4 μm (L_{M1} = 2 μm and L_{M2} = 2 μm) has a longer channel length than the SMG-based device. This result demonstrates that the effect of the DMG structure significantly increases carrier transport efficiency. The I_D of the DMG-based device gradually decreased as L_{M2} increased due to the increase in recess resistance. Thus, the DMG effect significantly reduced when L_G largely increased over 4 μm although the L_{M1}/L_{M2} ratio was small. In addition, the L_{M1}/L_{M2} ratio must be optimized to maximize the DMG effect because a short L_{M1} can be affected by short channel effects. The $I_{D,max}$ of the DMG-based device with L_G = 4 μm was also higher than that of the SMG-based device, as shown Figure 4b. The DMG structure considerably improved the channel resistance of the DMG-based device with L_G = 4 μm.

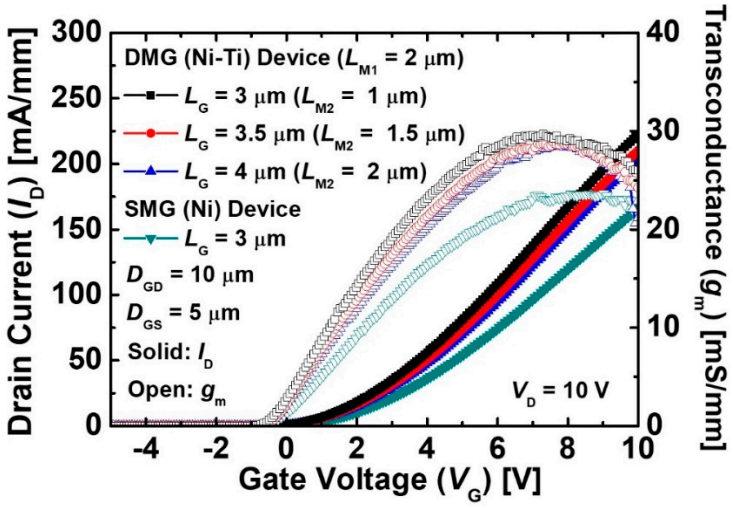

(**a**)

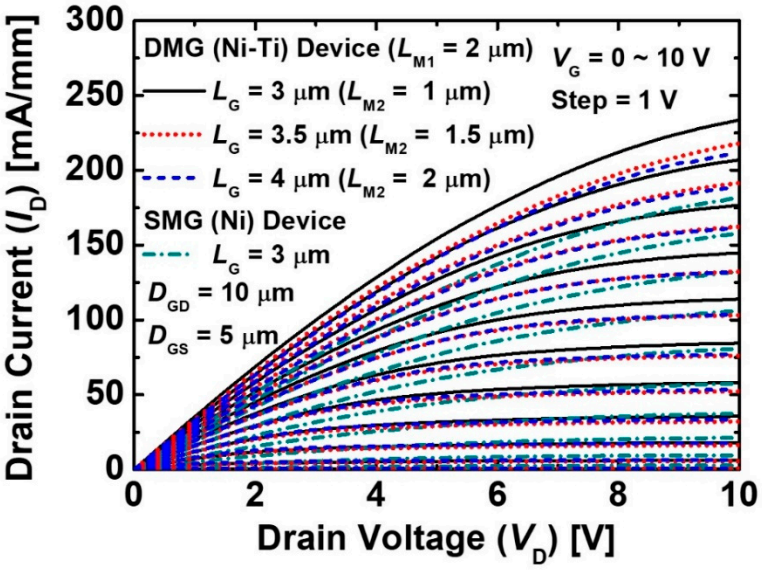

(**b**)

Figure 4. (**a**) Transfer and (**b**) output characteristics of the SMG- and DMG-based devices with different L_G. The D_{GD} and D_{GS} of both devices were 10 μm and 5 μm, respectively. The M1 and M2 in the DMG structure consist of Ni and Ti, respectively.

Furthermore, we investigated the effects of the work-function difference between the M1 and M2 on current characteristics. Figure 5 shows the transfer and output characteristics of the DMG (Ni-Al, Ni-Ti)- and SMG (Ni)-based devices. The DMG-based device with the Ni-Al improved I_D and g_m by 42.1% and 30.9%, respectively, compared to the SMG-based device. This result indicated that the effect of the DMG structure on current characteristics was further increased by a large work-function difference between the M1 and M2. The Ni-Al combination has a large electron potential difference because the work-function value of Al (about 4.1 eV) is lower than that of Ti (about 4.3 eV). The $I_{D,max}$ of the DMG-based device with Ni-Al was increased to 258.4 mA/mm, as shown in Figure 5b. The DMG structure with a large work-function difference improved carrier transport efficiency.

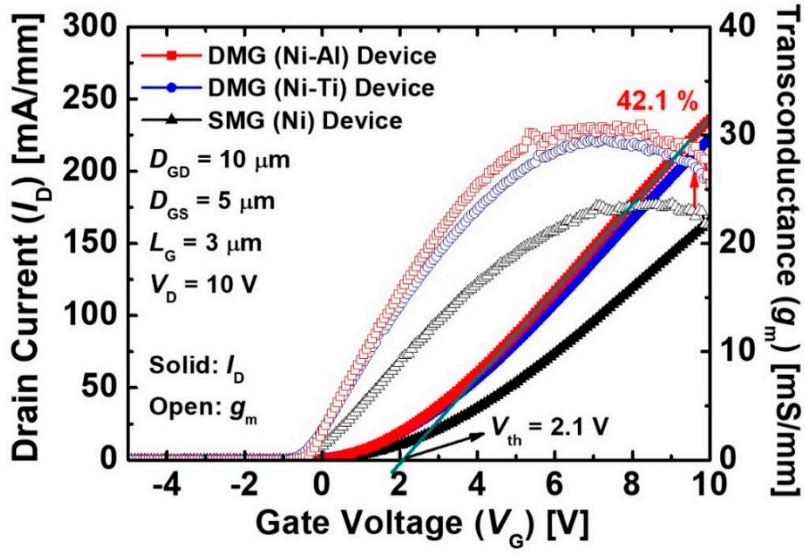

(**a**)

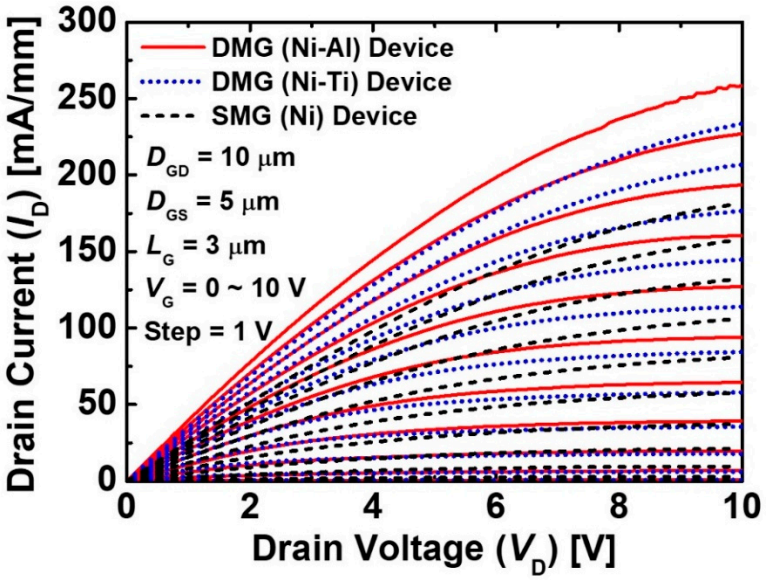

(**b**)

Figure 5. Effect of work-function difference in the DMG structure on current characteristics: (**a**) Transfer and (**b**) output characteristics of the devices with the SMG (Ni) and DMG (Ni-Al and Ni-Ti) structures. The L_G, D_{GD}, and D_{GS} of the devices were 3 μm, 10 μm, and 5 μm, respectively.

4. Conclusions

We fabricated GaN-based recessed-gate MOSFETs with the DMG structure and investigated the effects of DMG structure on the performances of recessed-gate MOSFETs. The fabricated device improved current characteristics because the DMG structure enhanced electron velocity under the gate region. The I_D and g_m of the DMG-based devices were higher than those of the SMG device, even though the L_G of the DMG-based devices was longer than that of the SMG-based device. A high V_{th} of the DMG-based devices was maintained by the work-function of the source-side metal. The device with the DMG (Ni-Al) structure achieved a higher $I_{D,max}$ of approximately 42% because the effects of the DMG structure on current characteristics were further enhanced by the large difference between work-functions in the DMG structure. As a result, the recessed-gate MOSFET using the DMG structure

simultaneously achieved excellent current characteristics and a high V_{th} without controlling the recess etching process.

Author Contributions: Conceptualization, Y.J.Y.; Investigation, Y.J.Y.; Data analysis, Y.J.Y., J.S.L., D.-S.K., J.-H.L. and I.M.K.; writing—original draft preparation, Y.J.Y.; writing—review and editing, I.M.K. All authors have read and agreed to the published version of the manuscript.

Funding: This work was supported by the National Research Foundation of Korea (NRF) grant funded by the Korea government (MSIT) (No. NRF-2020R1A2C1005087) and in part by Samsung Electronics Co. Ltd. The study was supported by the BK21 Plus project funded by the Ministry of Education, Korea (21A20131600011), by the Ministry of Trade, Industry & Energy (MOTIE) (10080513), and Korea Semiconductor Research Consortium (KSRC) support program for developing the future semiconductor devices. This work was also supported by the KOMAC (Korea Multi-purpose Accelerator Complex) operation fund of KAERI (Korea Atomic Energy Research Institute).

Conflicts of Interest: The authors declare no conflict of interest.

References

1. Mishra, U.K.; Parikh, P.; Wu, Y. AlGaN/GaN HEMTs—An overview of device operation and applications. *Proc. IEEE* **2002**, *90*, 1022–1031. [CrossRef]
2. Baliga, B.J. Gallium nitride devices for power electronic applications. *Semicon. Sci. Technol.* **2013**, *29*, 074011. [CrossRef]
3. Wu, Y.; Jacob-Mitos, M.; Moore, M.L.; Heikman, S. A 97.8% Efficient GaN HEMT Boost Converter With 300-W Output Power at 1 MHz. *IEEE Electron. Device Lett.* **2008**, *29*, 824–826. [CrossRef]
4. Wang, B.; Dong, S.; Jiang, S.; He, C.; Hu, J.; Ye, H.; Ding, X. A Comparative Study on the Switching Performance of GaN and Si Power Devices for Bipolar Complementary Modulated Converter Legs. *Energies* **2019**, *12*, 1146. [CrossRef]
5. Srivastava, P.; Das, J.; Visalli, D.; Hove, M.V.; Malinowski, P.E.; Marcon, D.; Lenci, S.; Geens, K.; Cheng, K.; Leys, M.; et al. Record Breakdown Voltage (2200 V) of GaN DHFETs on Si With 2-μm Buffer Thickness by Local Substrate Removal. *IEEE Electron. Device Lett.* **2011**, *32*, 30–32. [CrossRef]
6. Roccaforte, F.; Greco, G.; Fiorenza, P.; Iucolano, F. An Overview of Normally-Off GaN-Based High Electron Mobility Transistors. *Materials* **2019**, *12*, 1599. [CrossRef]
7. Saito, W.; Takada, Y.; Kuraguchi, M.; Tsuda, K.; Omura, I. Recessed-Gate Structure Approach Toward Normally OFF High-Voltage AlGaN/GaN HEMT for Power Electronics Applications. *IEEE Trans. Electron. Devices* **2006**, *53*, 356–362. [CrossRef]
8. Oka, T.; Nozawa, T. AlGaN/GaN Recessed MIS-Gate HFET With High-Threshold-Voltage Normally-Off Operation for Power Electronics Applications. *IEEE Electron. Device Lett.* **2008**, *29*, 668–670. [CrossRef]
9. Kim, K.-W.; Jung, S.-D.; Kim, D.-S.; Kang, H.-S.; Im, K.-S.; Oh, J.-J.; Ha, J.-B.; Shin, J.-K.; Lee, J.-H. Effects of TMAH Treatment on Device Performance of Normally Off Al_2O_3/GaN MOSFET. *IEEE Electron. Device Lett.* **2011**, *32*, 1376–1378. [CrossRef]
10. Kim, D.-S.; Im, K.-S.; Kang, H.-S.; Kim, K.-W.; Bae, S.-B.; Mun, J.-K.; Nam, E.-S.; Lee, J.-H. Normally-Off AlGaN/GaN Metal-Oxide-Semiconductor Heterostructure Field-Effect Transistor with Recessed Gate and p-GaN Back-Barrier. *Jpn. J. Appl. Phys.* **2012**, *51*, 034101. [CrossRef]
11. Asubar, J.T.; Kawabata, S.; Tokuda, H.; Yamamoto, A.; Kuzuhara, M. Enhancement-Mode AlGaN/GaN MIS-HEMTs With High V_{TH} and High I_{Dmax} Using Recessed-Structure With Regrown AlGaN Barrier. *IEEE Electron. Device Lett.* **2020**, *41*, 693–696. [CrossRef]
12. Hwang, I.; Kim, J.; Choi, H.S.; Choi, H.; Lee, J.; Kim, K.Y.; Park, J.-B.; Lee, J.C.; Ha, J.; Oh, J.; et al. p-GaN Gate HEMTs With Tungsten Gate Metal for High Threshold Voltage and Low Gate Current. *IEEE Electron. Device Lett.* **2013**, *34*, 202–204. [CrossRef]
13. Ge, M.; Ruzzarin, M.; Chen, D.; Lu, H.; Yu, X.; Zhou, J.; Santi, C.D.; Zhang, R.; Zheng, Y.; Meneghini, M.; et al. Gate Reliability of p-GaN Gate AlGaN/GaN High Electron Mobility Transistors. *IEEE Electron. Device Lett.* **2019**, *40*, 379–382. [CrossRef]
14. Huang, X.; Liu, Z.; Li, Q.; Lee, F.C. Evaluation and Application of 600 V GaN HEMT in Cascode Structure. *IEEE Trans. Power Electron.* **2014**, *29*, 2453–2461. [CrossRef]

15. Feng, Z.H.; Zhou, R.; Xie, S.Y.; Yin, J.Y.; Fang, J.X.; Liu, B.; Zhou, W.; Chen, K.J.; Cai, S.J. 18-GHz 3.65-W/mm Enhancement-Mode AlGaN/GaN HFET Using Fluorine Plasma Ion Implantation. *IEEE Electron. Device Lett.* **2010**, *31*, 1386–1388. [CrossRef]
16. Shen, F.; Hao, R.; Song, L.; Chen, F.; Yu, G.; Zhang, X.; Fan, Y.; Lin, F.; Cai, Y.; Zhang, B. Enhancement mode AlGaN/GaN HEMTs by fluorine ion thermal diffusion with high V_{th} stability. *Appl. Phys. Express* **2019**, *12*, 066501. [CrossRef]
17. He, J.; Hua, M.; Zhang, Z.; Chen, K.J. Performance and V_{TH} stability in E-Mode GaN Fully Recessed MIS-FETs and Partially Recessed MIS-HEMTs With LPCVD-SiN_x/PECVD-SiN_x Gate Dielectric Stack. *IEEE Trans. Electron. Devices* **2018**, *65*, 3185–3191. [CrossRef]
18. Son, D.-H.; Jo, Y.-W.; Won, C.-H.; Lee, J.-H.; Seo, J.H.; Lee, S.-H.; Lim, J.-W.; Kim, J.H.; Kang, I.M.; Cristoloveanu, S.; et al. Nomally-off AlGaN/GaN-based MOS-HEMT with self-terminating TMAH wet recess etching. *Solid State Electron.* **2018**, *141*, 7–12. [CrossRef]
19. Hahn, H.; Benkhelifa, F.; Ambacher, O.; Alam, A.; Heuken, M.; Yacoub, H.; Noculak, A.; Kalisch, H.; Vescan, A. GaN-on-Si Enhancement Mode Metal Insulator Semiconductor Heterostructure Field Effect Transistor with On-Current of 1.35 A/mm. *Jpn. J. Appl. Phys.* **2013**, *52*, 090204. [CrossRef]
20. Zhao, Y.; Wang, C.; Zheng, X.; Ma, X.; He, Y.; Liu, K.; Li, A.; Peng, Y.; Zhang, C.; Hao, Y. Effects of recess depths on performance of AlGaN/GaN power MIS-HEMTs on the Si substrates and threshold voltage model of different recess depths for the using HfO_2 gate insulator. *Solid State Electron.* **2020**, *163*, 107649. [CrossRef]
21. Wu, I.-L.; Tang, S.-W.; Jiang, H.-J. Investigation of Recessed Gate AlGaN/GaN MIS-HEMTs with Double AlGaN Barrier Designs toward an Enhancement-Mode Characteristics. *Micromachines* **2020**, *11*, 163. [CrossRef] [PubMed]
22. Long, W.; Ou, H.; Kuo, J.-M.; Chin, K.K. Dual-Material Gate (DMG) Field Effect Transistor. *IEEE Trans. Electron. Devices* **1999**, *46*, 865–870. [CrossRef]
23. Jang, Y.I.; Lee, S.H.; Seo, J.H.; Yoon, Y.J.; Kwon, R.H.; Cho, M.S.; Kim, B.G.; Yoo, G.M.; Lee, J.-H.; Kang, I.M. Design and Analysis of AlGaN/GaN MIS HEMTs with a Dual-metal-gate Structure. *J. Semicond. Technol. Sci.* **2017**, *17*, 223–229.
24. Jung, J.H.; Cho, M.S.; Jang, W.D.; Lee, S.H.; Jang, J.; Bae, J.-H.; Yoon, Y.J.; Kang, I.M. Fabrication of AlGaN/GaN MISHEMT with dual-metal gate electrode and its performances. *Appl. Phys. A* **2020**, *126*, 274. [CrossRef]
25. Tapajna, M.; Kuzmik, J. A comprehensive analytical model for threshold voltage calculation in GaN based metal-oxide-semiconductor high-electron-mobility transistors. *Appl. Phys. Lett.* **2012**, *100*, 113509. [CrossRef]
26. Lee, J.-Y.; Park, B.-R.; Lee, J.-G.; Lim, J.; Cha, H.-Y. Forming Gas Post Metallization Annealing of Recessed AlGaN/GaN-on-Si MOSHFET. *J. Semicond. Technol. Sci.* **2015**, *15*, 16–21. [CrossRef]
27. Ioannou-Sougleridis, V.; Karageorgiou, A.; Barlas, M.; Ladas, S.; Skarlatos, D. Interface properties of Al-Al_2O_3-Ge MIS capacitors and the effect of forming gas annealing. *Microelectron. Eng.* **2016**, *159*, 84–89. [CrossRef]
28. Zhang, L.; Guo, Y.; Hassan, V.V.; Tang, K.; Foad, M.A.; Woicik, J.C.; Pianetta, P.; Robertson, J.; McIntyre, P.C. Interface Engineering for Atomic Layer Deposited Alumina Gate Dielectric on SiGe Substrates. *ACS Appl. Mater. Interfaces* **2016**, *8*, 19110–19118. [CrossRef]
29. Fiorenza, P.; Greco, G.; Iucolano, F.; Patti, A.; Roccaforte, F. Channel Mobility in GaN Hybrid MOS-HEMT Using SiO_2 as Gate Insulator. *IEEE Trans. Electron. Devices* **2017**, *64*, 2893–2899. [CrossRef]
30. SILVACO. *ATLAS User's Manual*; SILVACO International: Santa Clara, CA, USA, 2000.
31. Ardaravicius, L.; Matulionis, A.; Liberis, J.; Kiprijanovic, O.; Ramonas, M.; Eastman, L.F.; Shealy, J.R.; Vertiatchikh, A. Electron drift velocity in AlGaN/GaN channel at high electric fields. *Appl. Phys. Lett.* **2003**, *83*, 4038–4040. [CrossRef]
32. Barker, J.M.; Ferry, D.K.; Koleske, D.D.; Shul, R.J. Bulk GaN and AlGaN/GaN Heterostructure drift velocity measurements and comparison to theoretical models. *J. Appl. Phys.* **2005**, *97*, 063705. [CrossRef]